Implementation of a collocated Boundary Element Method for acoustic wave propagation in multilayered fluid media

Elena Sundkvist Elisabeth Larsson

Abstract

The numerical solution of the Helmholtz equation with nonlocal radiation boundary conditions is considered. We model sound wave propagation in a multilayered piecewise homogeneous medium. A fourth-order accurate collocated, boundary element method is used, where the solution inside the domain is computed through a representation integral. The method is shown to have the expected fourth-order convergence and is also compared with a fourth-order accurate finite difference method.

1 Introduction

The boundary element method (BEM) is a powerful tool used for modelling various physical phenomena. For a comprehensive overview of the method we refer to the two volumes by Wrobel [26] and Aliabadi [1], where the theoretical development is presented as well as applications in various areas such as acoustics, electrochemistry, elastostatics, and elastodynamics. The application of BEM to acoustics is described and an overview of the literature is given for example in the books by Ciskowski and Brebbia [5], von Estorff [24], and Marburg [16].

In this research we are interested in sound wave propagation in a media consisting of several homogeneous layers. The waves are governed by the Helmholtz equation. A boundary integral equation technique based on [23] is employed, so the Helmholtz equation is used in its boundary integral form, where the solution inside the domain is represented through an integral involving the solution and the normal derivatives of the solution at the boundary. We assume axial symmetry of the domain so the problem is reduced to two dimensions and the boundary integrals become one-dimensional.

For computational purposes the domain is truncated, and artificial near- and far-field boundaries are introduced. Different boundary conditions can be used for such boundaries, as an example, perfectly matched layers can be mentioned [3, 22]. Here, the transparency of the vertical boundaries are modelled by employing nonlocal radiation boundary conditions, which to our knowledge have not been used with BEM before.

A fourth order accurate, collocated boundary element method is employed to discretize the integral formulation of the Helmholtz equation. A complete descrip-

tion of the method can be found in [21]. There, a hybrid model that couples the boundary integral equation and the Helmholtz differential equation is presented. Only the integral equation part is considered here.

Due to the wave nature of the solution, the number of grid points should follow the wavenumber. For higher frequencies when the wavenumber becomes large, or in case of large domains, more discretization points are needed. Even if for BEM only the boundaries are discretized, a high order method is of interest because it requires less grid points than a method of lower order. Most BEM implementations are first or second order accurate. For a special case of closed periodical boundary there are BEMs with spectral convergence [15, 7]. The collocated BEM constructed in [21] is shown here to be the fourth order accurate. The structure of the method is specified utilizing tensor notation. Through this framework, generalizations of the BEM to e.g. higher order of accuracy is facilitated.

However, in order to achieve the full order of convergence numerically, careful attention to some details is required. Integrals with singular kernels appearing from discretization of the integral equation, are studied in [21], where efficient quadratures for their numerical evaluation are proposed. Practical investigations of integrals with so called quasi-singular integrands are presented in Section 3.2.

The collocated, boundary element method is compared with a fourth order finite difference method (FD). The resolution in the FD method can not be based on a fixed number of elements per wavelength because of the phase error [2, 18]. For this BEM the phase error is not observed, for an illustration see Section 3.3. In Section 3.4 we compare memory requirements for FD and BEM. The methods have minor differences from this point of view, but for larger problems BEM uses less memory. Comparing the number of unknowns for FD and BEM we get the expected result, that the latter has more than an order of magnitude fewer unknowns.

The collocated BEM is realized in MATLAB, and the arising linear system of equations is solved by the standard built in Gaussian elimination procedure. This gives room for future investigations of more efficient solution procedures such as iterative methods.

The paper is structured as follows. In Section 2 the model problem is described. The entire Section 3 is devoted to numerical results. It consists of six subsections, where we analyze integrals with quasi-singular integrands, discuss phase error, memory requirements, resonance phenomenon, and show convergence of the collocated BEM. Finally, Section 4 contains conclusions and possible directions of future research.

2 The model problem

2.1 Physical problem and governing equations

We model sound wave propagation under water in a waveguide consisting of N homogeneous layers $\Omega_d, \quad d = 1, \ldots, N$. The subdomains can have different densities, sound speed and attenuation. Figure 1 illustrates an example of a cross-section of such a physical domain consisting of four subdomains with interface boundaries $\Gamma_2, \ldots, \Gamma_N$. The top boundary Γ_1 is horizontal to model the water surface. The vertical boundaries are artificial, they are added to make the

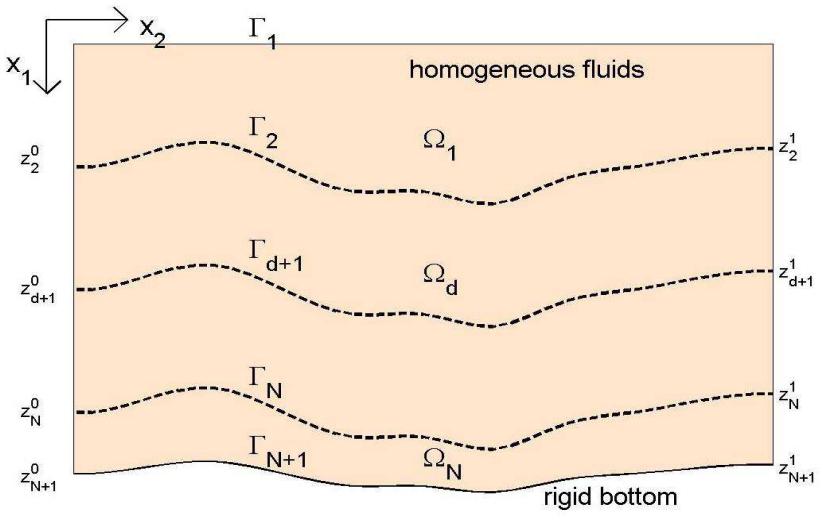

Figure 1: The physical domain.

problem numerically tractable.

The time-harmonic sound waves are governed by the Helmholtz equation

$$-\nabla \cdot \Big(\frac{1}{\varrho}\nabla p\Big) - \frac{\kappa^2}{\varrho}\, p = 0, \tag{1}$$

where $p(\boldsymbol{r})$ is the phasor of the acoustic pressure $\mathrm{Re}\big(p(\boldsymbol{r})\exp(-i2\pi f t)\big)$ and ϱ is the density [9, p. 73], [11, p. 12]. The wavenumber κ is given by $\kappa = \frac{2\pi f}{c}(1 + i\delta)$, where c is the sound speed, f is the frequency and δ is the loss tangent. If δ is nonzero then attenuation is presented.

Equation (1) is valid within each of the subdomains Ω_d where the density ϱ and the wavenumber are constant because the layers are homogeneous. In this case using Green's formula for equation (1), an integral representation of the solution $p(\boldsymbol{r}')$ can be derived at any field point $\boldsymbol{r}'$ in domain Ω_d resulting in

$$p_d(\boldsymbol{r}') = \int\limits_{S_d} \Big(G_d(\boldsymbol{r}', \boldsymbol{r})\frac{\partial p_d}{\partial n}(\boldsymbol{r}) - \frac{\partial G_d}{\partial n}(\boldsymbol{r}', \boldsymbol{r}) p_d(\boldsymbol{r})\Big)\, dS$$

where $G_d(\boldsymbol{r}', \boldsymbol{r})$ is the free-space Green's function [17, p. 805], $\frac{\partial}{\partial n} = \boldsymbol{n} \cdot \nabla$, and $\boldsymbol{n}$ is the outward unit normal of Ω_d at the boundary S_d.

In the limit where $\boldsymbol{r}'$ tends to the boundary, a so-called boundary integral equation (BIE) can be derived for the solution at the boundary [23, Sec. 2.5.4]:

$$\frac{1}{2}p_d(\boldsymbol{r}') + \int_{S_d} \Big(\frac{\partial G_d}{\partial n}(\boldsymbol{r}', \boldsymbol{r}) p_d(\boldsymbol{r}) - G_d(\boldsymbol{r}', \boldsymbol{r}) \frac{\partial p_d}{\partial n}(\boldsymbol{r}) \Big) \, dS = 0, \quad \boldsymbol{r}' \in S_d. \tag{2}$$

Thus, the solution inside Ω_d could be computed once the solution has been determined on the boundary S_d.

The problem is three-dimensional but here we assume plane symmetry, and work with a two-dimensional restriction of the problem. The field point $\boldsymbol{r}'$ is replaced by $\boldsymbol{x}' = (x_1', x_2')$. Then the far-field boundary is at $x_2 = r^1$ and the near-field boundary is at $x_2 = 0$.

There are no waves coming into the domain from outside so the outgoing waves only are admissible. The Green's function $G_d(\boldsymbol{x}', \boldsymbol{x})$ in this case are the zeroth order Hankel functions of the first kind [23, p. 177],[17, p. 623]:

$$G_d(\boldsymbol{x}', \boldsymbol{x}) = \frac{i}{4} \mathrm{H}_0^{(1)}(\kappa_d |\boldsymbol{x}' - \boldsymbol{x}|)$$

with normal derivatives given by

$$\frac{\partial G_d}{\partial n}(\boldsymbol{x}', \boldsymbol{x}) = \boldsymbol{n} \cdot \nabla G_d = \frac{i\kappa_d}{4} \mathrm{H}_1^{(1)}(\kappa_d |\boldsymbol{x}' - \boldsymbol{x}|) \frac{(\boldsymbol{x}' - \boldsymbol{x}) \cdot \boldsymbol{n}}{|\boldsymbol{x}' - \boldsymbol{x}|}.$$

2.2 Boundary and interface conditions

In addition to equations (2), boundary and interface conditions are needed in order to couple the solutions between neighboring domains. We employ conditions similar to the ones used in [21], but with Neumann type at the bottom. That means that on the surface boundary Γ_1, pressure release is imposed. On the interfaces between the layers, the pressure and the normal velocity are required to be continuous, and at Γ_{N+1} the hard rock is modelled, i.e.

$$\begin{cases} p_1(\boldsymbol{x}) = 0, \quad \boldsymbol{x} \in \Gamma_1 \\ p_d(\boldsymbol{x}) = p_{d+1}(\boldsymbol{x}), \qquad \boldsymbol{x} \in \Gamma_{d+1}, \ d = 1, \ldots, N-1, \\ \frac{1}{\varrho_d} \frac{\partial p_d}{\partial n}(\boldsymbol{x}) = \frac{1}{\varrho_{d+1}} \frac{\partial p_{d+1}}{\partial n}(\boldsymbol{x}), \ \boldsymbol{x} \in \Gamma_{d+1}, \ d = 1, \ldots, N-1, \\ \frac{\partial p_N}{\partial n}(\boldsymbol{x}) = 0, \ \boldsymbol{x} \in \Gamma_{N+1}. \end{cases} \tag{3}$$

2.3 Radiation boundary conditions

The artificial far-field and near-field boundaries should be transparent to all waves. We emulate this by employing the same nonlocal Dirichlet-to-Neumann

(DtN) maps as were used in [21] on the base of [10] and [12, p. 1720]. The sound waves emanate from a truncated point source located at the left boundary leading to the DtN conditions there

$$(4)\quad -\frac{\partial p}{\partial x_2}(x_1,0) - \sum_{m=1}^{\mu_0} i\sqrt{-\lambda_m^0}\langle\psi_m^0, p(\cdot,0)\rangle\psi_m^0(x_1) = -\sum_{m=1}^{\mu_0} 2i\sqrt{-\lambda_m^0}A_m\psi_m^0(x_1),$$

for $0 \le x_1 \le z_{N+1}^0$. At the right boundary we have

$$(5)\qquad \frac{\partial p}{\partial x_2}(x_1,r^1) - \sum_{m=1}^{\mu_1} i\sqrt{-\lambda_m^1}\langle\psi_m^1, p(\cdot,r^1)\rangle\psi_m^1(x_1) = 0,$$

for $0 \le x_1 \le z_{N+1}^1$. The coefficients A_m are known and characterize the source, and μ_0, μ_1 are the cutoff limits. The eigenmodes $\psi_m^b(x_1)$ and the corresponding eigenvalues λ_m^b are solutions of Sturm-Liouville problems at the near- and far-field boundaries, $b = 0, 1$. The eigenfunctions ψ_m are conjugate with respect to the bilinear form

$$\langle f, g\rangle \equiv \int_0^{z_{N+1}} \frac{1}{\varrho}\, f(z)g(z)\, dz,$$

which means that $\langle\psi_m, \psi_n\rangle = \delta_{mn}$.

Boundary conditions based on DtN maps require the boundary in question to be a separable coordinate surface. The Helmholtz equations (1) can be solved by separation of variables *beyond* each artificial boundary under the assumption that the wavenumber κ depends on the depth only and that the bathymetry is horizontally stratified. The solution in case of plane symmetry is [21, Sec. 3]:

$$(6)\qquad p(x_1,x_2) = \sum_{m=1}^{\mu} A_m\,\psi_m(x_1)\exp(i\sqrt{-\lambda_m}x_2).$$

For the case of a homogeneous domain with horizontal boundary Γ_{N+1} the modes can be calculated analytically and the solution is following:

$$(7)\qquad p(x_1,x_2) = \sum_{m=1}^{\mu} A_m\sqrt{2\rho/z_{N+1}^0}\sin((m-1/2)\pi x_1/z_{N+1}^0))\exp(i\sqrt{-\lambda_m}x_2)$$

with $\lambda_m = ((m-1/2)\pi/z_{N+1}^0)^2 - \kappa^2$. Formulas (6) and (7) will be used for calculating reference solutions for the corresponding problems.

2.4 Discretization

We will briefly describe the discretization of the continuous problem consisting of the BIEs (2) for each domain Ω_d and the boundary conditions (3)–(5). The discretization approach is described in more detail in [21]. The difference concerns the bottom boundary Γ_{N+1} which was excluded of the discretization process because of the absorbing boundary conditions. Here it is treated the same way as the other interfaces. All equations are discretized by fourth-order accurate methods.

In the boundary integral method we discretize only the boundaries and can have different numbers of points for different boundary segments of a domain. We have $m_{\frac{1}{2},d} + 1$ points on Γ_d, $d = 1, \ldots, N+1$, and $m_{b,d} + 1$ (here equidistant) points on the left and right artificial boundaries $x_1 \in [z_d^b, z_{d+1}^b]$, $b = 0, 1$, $d = 1, \ldots, N$ of domain Ω_d. The number of intervals are $m_{\frac{1}{2},d}$ and $m_{b,d}$ correspondingly. Approximants of the pressure and the normal derivatives at each interval are represented as linear combinations of four basis functions. The basis functions are piecewise linear functions $\widehat{\varphi}_{j,1}(t)$ with support on the two intervals j and $j+1$, and integrated piecewise Legendre polynomials $\widehat{\varphi}_{j,2}(t)$, $\widehat{\varphi}_{j,3}(t)$, which have support only on element j.

To determine the coefficients for the approximants a collocation method is employed. The boundary integral equations are collocated at two equidistant points inside every applicable element and at every applicable node point except at the artificial corners $x_1 = z_d^b$, $d = 1, \ldots, N+1$, $b = 0, 1$. The DtN conditions (4)–(5) are collocated at the two points inside every applicable element and at every applicable node point including $x_1 = z_{N+1}^b$, $b = 0, 1$.

In the arising linear system the coefficients have the form of one-dimensional integrals which can be calculated numerically. The integrals corresponding to one discretizaton interval are called element integrals. The integrands of the element integrals are the Green's functions, which are Hankel functions of the first kind in the case of plane symmetry, or the Green's function's normal derivatives, multiplied by the polynomial basis functions. The element integrals are calculated with three point Gauss-Legendre quadrature. When the collocation point belongs to the integration interval the integrand becomes singular. Therefore, we require the construction of a special quadrature where three point Gauss-Legendre quadrature for integrals with logarithmic singularities is employed [21, Sec. A.2], [6]. Nonsingular integrands being close to a singularity are called quasi-singular and the integrals with such integrands are calculated with composite three point Gauss-Legendre quadrature. They are discussed further in Section 3.2.

3 Numerical results

3.1 The test problems

The following three types of test problems are used in all the performed experiments of this section. The waveguide consists of N layers and has hard rock at the bottom. The source is located in the top water domain at 20 m depth. The wavenumber κ is given by $\kappa_d = \frac{2\pi f}{c_d}(1 + i\delta_d/(40\pi \log_{10} e))$. If it is not specially pointed out, the frequency is 25 Hz, the length of the channel is 600 m and the number of layers $N = 3$. In all performed tests the source is truncated so that at most five modes are taken into consideration, i.e., the coefficients A_m from (4) are equal to zero for $m > 5$.

Test problem 1. If we have water in all layers the problem is identical to a one-layer problem. For a horizontal bottom curve Γ_{N+1} it can be solved analytically. The reference solution can be found through (7). The artificial interface boundaries Γ_d for $1 \leq d \leq N$ are curved.

Test problem 2. In case of different media but with all Γ_d horizontal the solution can be found through (6). Attenuation in at least the Nth layer is nonzero. To build the reference solution, the Sturm-Liouville problem mentioned in Section 2.3 is solved on a very fine grid such as 50 grid intervals per wavelength.

Test problem 3. In the third test problem we have layers with different media, curved interfaces and attenuation in the last domain. As reference solution in this case we use the BEM solution of the problem calculated with high resolution such as 50 intervals per wavelength.

Table 1: Examples of parameters used in the numerical experiments.

layer	density kg/m^3	sound speed m/s	absorbtion δ_d	depth left	depth right
The first problem: artificial interfaces, curved Γ_d for $1 \leq d \leq N$					
1	1000	1500	0	145	100
2	1000	1500	0	220	260
3	1000	1500	0	410	410
The second problem: all Γ_d are horizontal					
1	1000	1500	0	145	145
2	1200	1700	0	220	220
3	2700	4000	0.8	410	410
The third problem: Γ_d are curved for $d > 1$					
1	1000	1500	0	145	100
2	1200	1700	0	220	260
3	2700	4000	0.8	410	380

3.2 Convergence issues

The discretization described in Section 2.4 is fourth order. However, in order to achieve fourth order convergence numerically, careful attention to some details is required.

Quasi-singular integrands. Let us consider a typical element integral:

$$\int_{S_j} \mathrm{H}_0^{(1)}(\kappa_d|\boldsymbol{x}' - \boldsymbol{x}|)\varphi(s)\, dS_j, \quad \boldsymbol{x} \in S_j, \tag{8}$$

where the collocation point $\boldsymbol{x}'$ belongs to the same boundary (for example Γ_2) as the integration interval S_j and $\varphi(s)$ is a basis function over the element j.

The integrands can be singular or non-singular. Using the Lachat-Watson transformation and Taylor expansion it is shown that integral (8) has a logarithmic type of singularity if $\boldsymbol{x}' \in S_j$ [21, Sec. A.2]. In this case integral (8) is calculated with a special three-points Gauss-Legendre quadrature for logarithmic singularities [6].

If the element integrals for all nonsingular integrands are calculated by three point Gauss-Legendre quadrature, the solution of the whole problem has less than linear convergence. It is due to the error in the calculation of integrals when the collocation point $\boldsymbol{x}'$ does not belong to, but is close to, the integration interval S_j.

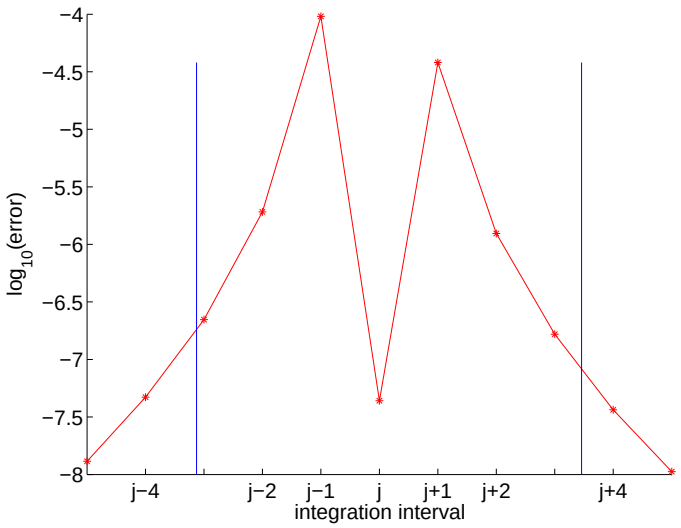

Figure 2: Error in calculation of element integrals. The vertical lines mark a distance of 0.15 wavelengths from the (non-symmetrical) collocation point

Figure 2 shows an example of the error in element integrals around a collocation point belonging to the integration interval S_j on the curved boundary Γ_2. The

results calculated by the applicable three point Gauss-Legendre quadrature are compared with results calculated by the composite trapezoidal rule with a very large number of subintervals. The errors are small for the singular integral over S_j and for the non-singular integrals $S_{j\pm4}$. For the integrals $S_{j\pm1,2}$ we observe obvious peaks. The ordinary three points Gauss-Legendre quadrature does not work well enough in this case because Hankel functions are badly approximated by polynomials close to the singularity. The integrands of such integrals are called quasi-singular. By numerical experiments we established that the integrals need special treatment in the problem settings we are interested in, when the distance between a collocation point and an integration interval $|\boldsymbol{x}' - \boldsymbol{x}|$ is less then 0.15λ. The wavelength λ depends on the material and is computed as c_d/f. This distance is marked with the vertical lines in Figure 2. The lines are not symmetric because the collocation point is not symmetrically placed in the interval.

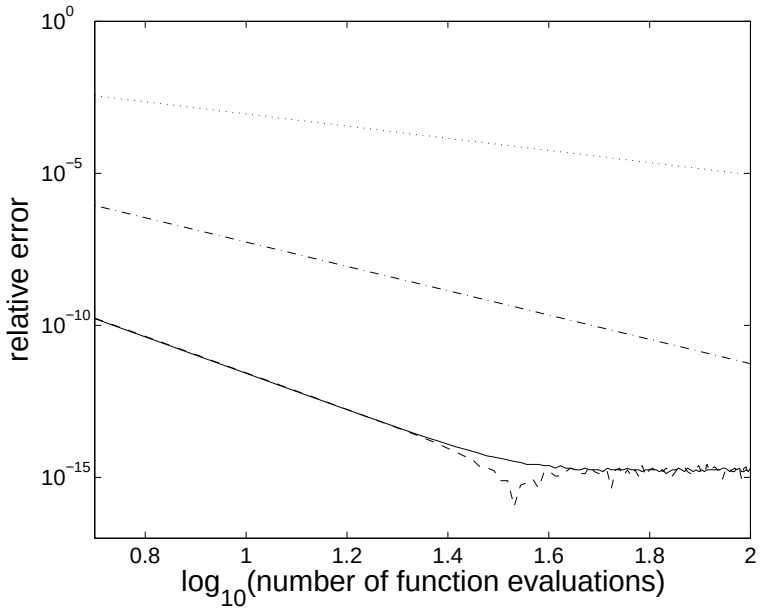

Figure 3: Performance of Midpoint (dotted), Simpson's (dash dotted), composite closed Newton-Cotes with 4 points (dashed) and Composite three points Gauss-Legendre (solid) quadratures for quasi-singular integrals with logarithmic singularity.

A suitable model problem to test different quadratures and choose the best one for calculation of the quasi-singular integrals is numerical calculation of the integral $\int_{-1}^{1} \log(0.5(s+1)+q)\varphi(s)\,ds$, where $\varphi(s)$ is a local basis function and $q = 1, 2, 3$ is the index of the collocation point [21, Sec. A.2.2]. We tested four quadratures for all four basis functions and all q. In Figure 3, the relative error is plotted against the number of function evaluations for $\varphi_2(s) = 0.5(1-s)$ and $q = 2$. Composite three point Gauss-Legendre quadrature performs best, therefore we employ it for the calculation of integrals with quasi-singular integrands. By

numerical experiments we found that eight composite intervals is sufficient to get the same range of error as in all others integrals. When the collocation points are further from the integration interval, fewer intervals would suffice, but we did not employ adaptivity because the quadrature is so fast.

The obvious cases of integrals with quasi-singular integrands are when $\boldsymbol{x}'$ and $\boldsymbol{x}$ belongs to the same boundary or to neighbor boundaries near corners. A less obvious case is when two interface boundaries Γ_d and Γ_{d+1} become too close to each other. This case is not handled by the current implementation but could be added without too much effort.

Interfaces near artificial boundaries When modelling the interfaces Γ_d one *must* have them horizontal at the artificial near- and far-field boundaries. It is implicitly assumed that the normal derivative of the pressure $\frac{dP}{dx_1}$ is aligned with the vertical direction at the artificial corners because any bias introduces a permanent error that ruins convergence of the whole solution. We use the following trigonometric curves $x_1(t) = d + \frac{a}{2}(1 - \cos(C\pi t))$, where $0 \le t \le 1$, constant C is an integer number (usually odd), and parameters d and a define depth on the near-field boundary and the maximum depth change (positive or negative) correspondingly.

3.3 Phase error

The solutions of problem (2) are wave functions so the resolution should follow the wavelength λ in corresponding direction, see previous section 3.2. The number of grid intervals in each domain is based on a fixed number of intervals per wavelength. In finite difference and finite element methods this approach does not work because of phase error. It grows in the propagation direction and is proportional to $f^{p+1}h^p$ for a p-th order method [2, 18, 8], where f is the frequency and h is the grid size for a given problem.

To study this phenomenon for BEM we can either increase the length of the channel making the frequency higher in relation to the length scale or increase the frequency. We choose the second way and solve the test problems 1–3 from Section 3.1 with fixed channel length equal to 300 m. For the first and the second problems, where we can easily get the reference solution, the frequency varies from 25 to 100 Hz. For the third problem, where we need to calculate the reference solution by solving the problem with very high resolution, it becomes too time and memory consuming. The relative L_2 error on the near- and far- field boundaries $[z_1^0\ z_{N+1}^0]$, $[z_1^1\ z_{N+1}^1]$ for problems 1–3 is presented in Figure 4 for the corresponding frequencies. It is clearly seen in the figure that with increased frequency the error remains nearly constant for all three problems on both boundaries. It does not grow in the propagating direction which means that the effect of phase error is not observed. Therefore a fixed number of grid intervals per wavelength is a proper base for the resolution when we use the BEM.

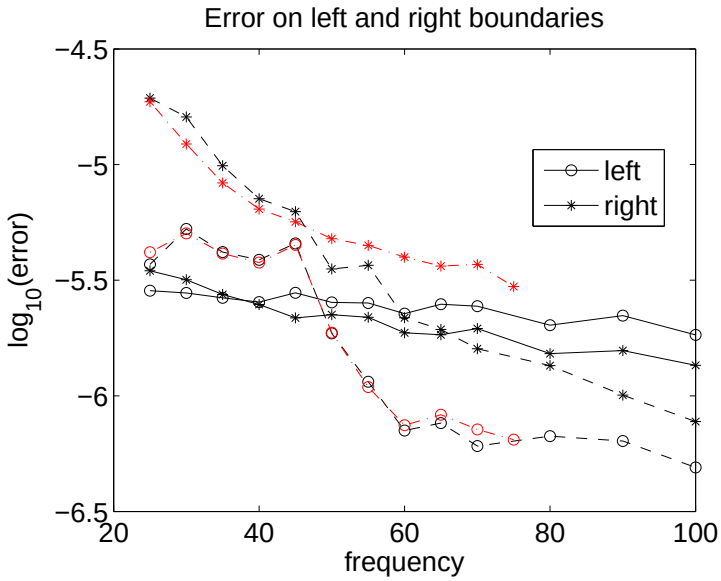

Figure 4: The relative errors on the near- (∘) and far-field (*) boundaries depending on frequency for the first (solid), second (dashed) and the third (dash-dotted) test problems.

3.4 Memory requirements

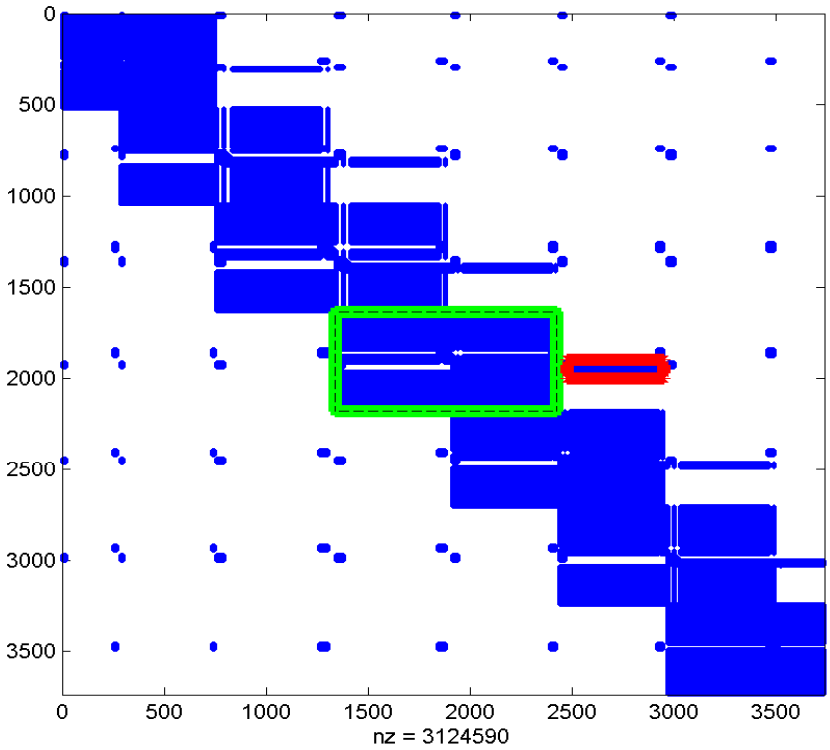

Figure 5: The structure of the matrix B for a problem with 7 domains.

Here we discuss memory requirements of the method. On each boundary β of domain Ω_δ we have $m_{\beta,\delta}$ integration intervals. Typically, six unknowns correspond to each interval so on each boundary there are $6m_{\beta,\delta}$ unknowns. Some of them are eliminated because of the boundary and compatibility conditions. We introduce the following variables

$$m_\beta = \sum_{\delta=1}^{N} m_{\beta,\delta},\ \beta = 0, 1,\ \delta = 1, \ldots, N \quad \text{and} \quad m_2 = m_{\frac{1}{2},\delta},\ \delta = 1, \ldots, N+1.$$

Notice that the resolution in the x_2 directions is the same for all domains. The number of unknowns in the BEM $n_{sol} = 6(m_0 + Nm_2 + m_1) - 2N$. The matrix of the system of equations arising from discretization of the numerical problem (2), called B, has block structure as shown in Figure 5. The test problem in this case consists of seven domains. For one domain the matrix is nearly dense. The matrix becomes more sparse for problems with more domains because only the neighbor domains are connected through the boundary integral equations and the contribution of the DtN conditions is minor. On the other hand the size of the matrix grows for more domains.

We denote the number of unknowns corresponding to the domain Ω_δ by n_δ. The unknowns belongs to the vertical and the top boundaries of the domain. Then

$$n_\delta = \begin{cases} 6(m_{0,\delta} + m_{1,\delta}) + 3m_2 - 5 & \text{for } \delta = 1, \\ 6(m_{0,\delta} + m_2 + m_{1,\delta}) - 2 & \text{for } \delta = 2, \ldots, N-1 \\ 6(m_{0,\delta} + m_2 + m_{1,\delta}) + 2 & \text{for } \delta = N, \\ 3m_2 - 1 & \text{for } \delta = N+1, \end{cases}$$

and the size of the nearly dense diagonal block surrounded by the green rectangle is $(6(m_{1,\delta} + m_2 + m_{0,\delta+1}) - 2)(n_\delta + n_{\delta+1})$ for $\delta = 4$. The block surrounded by the red rectangle corresponds to the continuity conditions on the bottom interface boundary of the domain $\Omega_{\delta+1}$, i.e. $\Gamma_{\delta+2}$, and has width $n_{\delta+2}$. It occupies less positions than the zeros in the big block.

The small blocks outside the diagonal correspond to the DtN conditions which need $n_{DtN} = 9(m_0^2 + m_1^2)$ positions. The number of nonzero elements of the matrix B can be estimated as

$$n_B \leq (n_1 + 3m_2 + m_{0,2} - 1)(n_1 + n_2) + \sum_{\delta=2}^{N-1} 6(m_{1,\delta} + m_2 + m_{0,\delta+1})(n_\delta + n_{\delta+1}) + \ldots$$

$$6(m_{1,N} + m_2)(n_N + n_{N+1}) + n_{DtN}.$$

To simplify it even more we suppose $m_{0,\delta} = m_{1,\delta} = m_1$, then n_B can be estimated as $n_B \leq 72((N - 1/2)(2m_1 + m_2)^2 - m_1^2)$.

A benefit of using BEM is that we only discretize the boundary. To study the effect in terms of memory requirements and number of unknowns needed, we compare with a FD method.

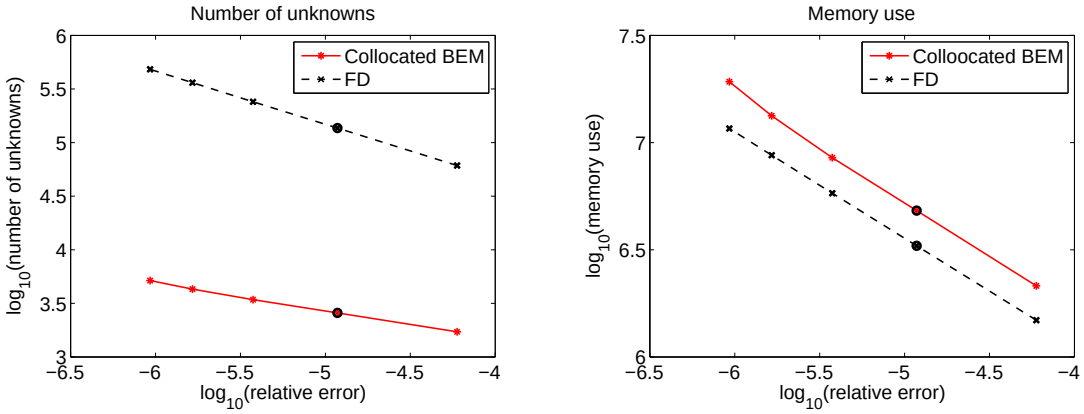

Figure 6: Number of unknowns (left) and memory usage (right) depending on resolution for FD (dashed) method and for BEM (solid)

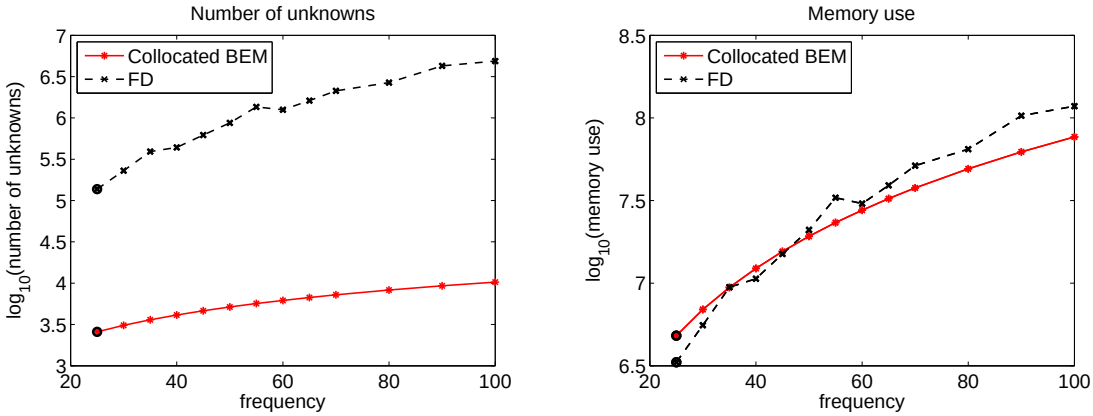

Figure 7: Number of unknowns (left) and memory use (right) depending on frequency for FD (dashed) and BEM (solid)

In the FD method the whole domain is discretized so the number of unknowns in BEM is much less than in FD. We should notice here that to reach the same accuracy the number of intervals $m_{\beta,d}$ and m_2 are different for the different methods. In the FD case there are [13, p. 6] specific formulas to find the resolution to get a given tolerance. If we consider a rectangular domain, i.e., with the same number of intervals on the left and right side, then in our variables they are the following:

$$h_{1,d}^{FD} \leq \frac{(480 \max(r_3\sqrt{-\lambda_\mu}, \frac{1}{5})\tau)^{1/4}}{\sqrt{r_3\kappa_d^3}(z_d - z_{d-1})}, \quad m_{1,d}^{FD} = \left\lceil \frac{1}{h_{1,d}} - \frac{1}{2} \right\rceil,$$

$$h_2^{FD} = \frac{(480\tau)^{1/4}}{(\sqrt{-\lambda_1}r_3)^{5/4}}, \qquad m_2^{FD} = \left\lceil \frac{1}{h_2} + 2 \right\rceil.$$

We do not have such formulas in boundary integral method. Therefore, to compare the two methods from a memory point of view, we first run the integral

method and compute the error τ. Then we calculate the resolution for FD using the given formulas and calculate the memory requirements for the found $m_{1,d}^{FD}$ and m_2^{FD} as in [13, paper IV, p. 15].

Figures 6 shows a comparison of memory requirements and numbers of unknowns for the FD and BE methods used for test problem 1 from section 3.1 with the length of the channel equal to 300 m and different resolutions. The frequency is constant and equal to 25 Hz. The number of unknowns in BEM is more than one order of magnitude less than in FD but the method requires more memory. The frequency and, correspondingly, the problem are small and such small errors are typically not necessary in real calculations. This example is just to show that the memory requirements grow with the same rate in both methods. We are more interested in how the methods perform for larger problems.

When the resolution is fixed, but the frequency grows, the number of unknowns and memory requirements are shown in Figure 7. Again, as expected, the number of unknowns is much less for the boundary integral method and for larger problems the difference grows. The memory requirements are comparable but we can see that for higher frequencies the boundary integral method uses less memory than FD. The circles in Figures 6 and 7 mark the common conditions for the two tests, i.e., $f = 25$ Hz and resolution 15 grid intervals per wavelength. This is done to show order of the error in the second test which is not obvious from the figure.

3.5 Resonance

The DtN conditions from section 2.3 are constructed for waves that propagate. For a standing mode the DtN condition (4) can not define the coefficients a_M and b_M in $p(x_1, x_2) = \sum_{m=1}^{\mu} \psi_m(x_1)(a_m \exp(i\sqrt{-\lambda_m}x_2) + b_m \exp(-i\sqrt{-\lambda_m}x_2))$ because the corresponding propagation constant λ_M is equal to zero.

This happens, for example, for the Mth mode in case of a rectangular domain without attenuation when the frequency $f = 0.5(M - 0.5)c/z$, where c is the sound speed and z is the depth. The boundary integral method leaves the resonant mode undetermined in this case. It is clear from Figure 8 that the performance is not satisfactory. We calculate the scaled L_2 error in the solution of the boundary integral method and find the maximum of the errors over all boundaries. The maximum L_2 error for a test problem with resonance at 25 Hz is plotted against frequency in Figure 8. Of course, we can perturb the physical problem, i.e., slightly change the frequency, the depth or media properties, but a more sober approach is to modify the boundary conditions so that they handle standing modes.

1. First of all we need to make the mode solver robust so that it finds the standing mode. We make an assumption that all modes with a very small absolute value of the eigenvalue are treated as standing and explore the absolute value of the error

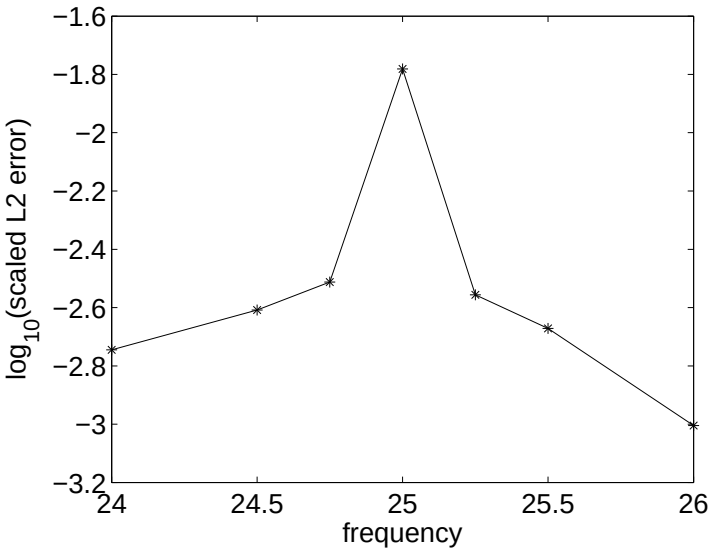

Figure 8: Error as a function of frequency for a problem with three layers with equal parameters $c = 1500$, $\rho = 1000$ and without attenuation. The straight bottom is at 135 m depth. We use 12 discretization intervals per wavelength.

between the truly standing mode with the propagation constant equal to zero and an approximately standing mode with the propagation constant $\sqrt{-\lambda_m} = \beta$ being small. The relative error of the standing mode solution $\psi_m e^{i0x_2}$ compared with the weakly propagating mode solution $\psi_m e^{i\beta x_2}$ can be measured as

$$|e^{i0x_2} - e^{i\beta x_2}| \leq \tau.$$

For a small β, this quantity grows linearly, i.e., the maximum value is attained at the largest x_2-value

$$|1 - e^{i\beta z}| = \sqrt{(1 - \cos(\beta z))^2 + \sin(\beta z)^2} = \sqrt{2 - 2\cos(\beta z)} \approx \beta z.$$

The condition for a numerically standing mode becomes

$$|\beta| \leq \frac{\tau}{z}.$$

This means that in the mode solver, eigenvalues fulfilling this can be treated as standing in the DtN condition with propagation constant $\beta = 0$.

2. The second step is to modify the DtN conditions for the near-field boundary for the standing mode. To define the amplitude of the standing mode we introduce the condition

$$\langle \psi_M^0, p(\cdot, 0) \rangle = A_M \tag{9}$$

and by exploiting the orthogonality of the eigenfunctions ψ_m (see Section 2.3) enforce $b_M = 0$. Modifying the coefficients in (4) according to (9) for the standing

mode gives the following DtN condition for the near-field boundary
(10)

$$-\frac{\partial p}{\partial x_2}(x_1,0)+\sum_{m=1}^{\mu_0} C_m^0\langle\psi_m^0,p(\cdot,0)\rangle\psi_m^0(x_1)=\sum_{m=1}^{\mu_0} A_m^0\psi_m^0(x_1),\quad 0\le x_1\le z_{N+1}^0,$$

where $C_m^0=-i\sqrt{-\lambda_m^0}$, $A_m^0=-2i\sqrt{-\lambda_m^0}A_m$ for $m\neq M$ and $C_M^0=1$, $A_M^0=A_M$.

3. If the standing mode exists and is not included in the DtN conditions because of the cut-off criterium μ_b it still introduces problems in the solution. Then we need to solve the Sturm-Liouville problem again to resolve the standing mode and modify the DtN conditions for it.

This algorithm has not been implemented and numerically tested yet.

3.6 Convergence results

We choose to check convergence of the collocated BEM on the three types of test problem from Section 3.1 because they cover a range of combinations that the boundary integral method can be used for.

Knowing the analytical solution in problem1, where the media in different layers is the same and the bottom boundary is straight, we check that the boundary conditions are done properly.

The second test problem checks how the method works for different layers and for nonzero attenuation in rectangular domains.

And the third test problems is the type of real problem we intend to solve with our method, i.e. all boundaries Γ_d, $d=1,\ldots,N$ are curved, the media is different in different layers and attenuation is nonzero.

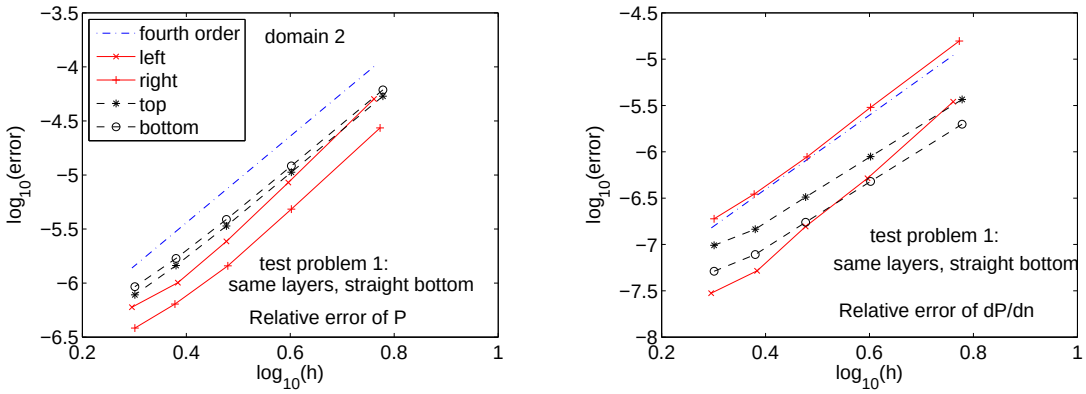

Figure 9: Problem 1: Relative error of solution (left) and it's normal derivatives (right) on all boundaries of the second domain. The resolution is 10, 15, 20, 25, 30 discretization intervals per wavelength.

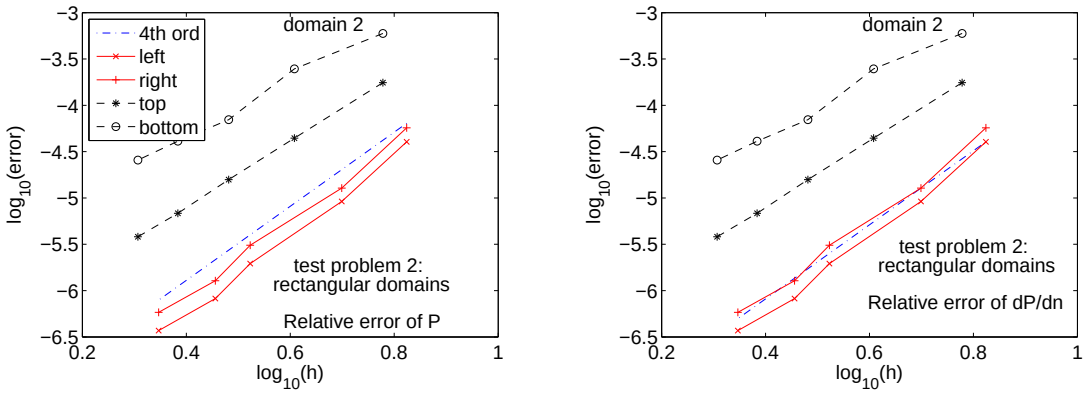

Figure 10: Problem 2: Relative error of solution (left) and it's normal derivatives (right) on all boundaries of the second domain. The resolution is 10, 15, 20, 25, 30 discretization intervals per wavelength.

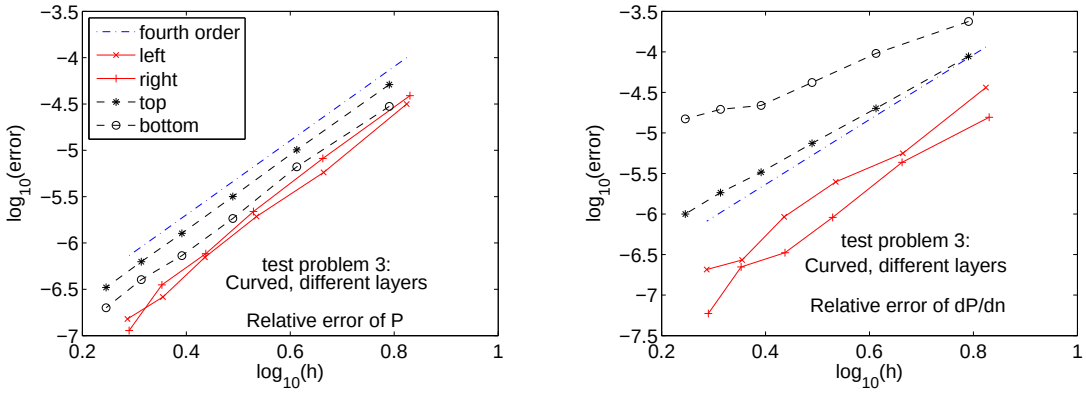

Figure 11: Problem 3: Relative error of solution (left) and it's normal derivatives (right) on all boundaries of the second domain. The resolution is 10, 15, 20, 25, 30, 35 discretization intervals per wavelength.

Figures 9–11 demonstrate the convergence of the relative error of the solution and the normal derivatives in L_2-norm on the boundaries of the middle layer. The boundary integral method solutions show fourth order convergence in all cases.

The normal derivative exhibits fourth order of convergence along straight boundaries including the interfaces in problem 2. Curved boundaries cause a drop in convergence. The reason why this happens is not clear yet and needs further investigations.

We get nearly the same curves for the convergence of the solution and the normal derivative on the boundaries of the other layers.

4 Conclusions

In this article a fourth order accurate collocated, boundary element method is implemented for a layered domain, using nonlocal radiation boundary conditions for the artificial vertical boundaries. The method was introduced in [21]. Here it is briefly described and tested numerically. The method is fourth order accurate. To our knowledge, this has not been achieved before for these types of methods. The memory requirements of the method are also compared with the memory requirements of the fourth order finite difference method from [14]. Both methods require nearly the same amount of memory but for larger problems the collocated BEM becomes better. The number of unknowns in the BEM is noticeably less, which makes the method attractive from a numerical point of view.

The method is implemented in MATLAB so far, using a direct method for solution of the linear system of equations arising from the discretization. For one layer the matrix of this system is dense but when the number of layers grows, it becomes more sparse, see Figure 5. One of the directions for future research is construction and implementation of a suitable iterative method for solution of the system of equations. Another direction is to implement the BEM in FORTRAN, and then the hybrid method which is fully described in [21].

Acknowledgments. The first author would like to thank her advisor Docent Kurt Otto and Docent Maya Neytcheva for valuable suggestions about the implementation of the BEM.

References

[1] M. H. ALIABADI, *The boundary element method. Volume 2. Applications in Solid Structures*, John Wiley&Sons, LTD, 2002.

[2] A. BAYLISS, M. GUNZBURGER, AND E. TURKEL, *On accuracy conditions for the numerical conditions of waves*, J. Comput. Phys., 59 (1985), pp. 396–404.

[3] J. P. BERENGER, *A perfectly matched layer for the absorption of electromagnetic waves*, J. Comput. Phys. 114 (1994), pp. 185-200.

[4] D. K. CHENG, *Field and Wave Electromagnetics*, Addison–Wesley, Reading, MA, 2nd ed., 1989.

[5] R. D. CISKOWSKI, C. A. BREBBIA, eds., *Boundary elements in acoustics*, Computational Mechanics Publications and Elsevier Applied Science, Southampton, 1991.

[6] L. GAUL, M. KÖGL, M. WAGNER, *Boundary Element Methods for Engineers and Scientists*, Springer-Verlag Berlin Heidelberg, 2003.

[7] F. Q. Hu, *A spectral Boundary Integral Equation Method for the 2D Helmholtz Equation*, J. Compu. Phys. 129 (1995), No. 2, pp. 340–347.

[8] F. Ihlenburg and Babušhka, *Finite element solution of the Helmholtz equation with high wave number Part II: the h-p version of the FEM*, SIAM J. Numer. Anal., 34 (1997), pp. 315–358.

[9] F. B. Jensen, W. A. Kuperman, M. B. Porter, and H. Schmidt, *Computational Ocean Acoustics*, AIP Press, New York, 1994.

[10] J. B. Keller and D. Givoli, *Exact non-reflecting boundary conditions*, J. Comput. Phys., 82 (1989), pp. 172–192.

[11] S. Kirkup, *The boundary Element Method in Acoustics. A development in Fortran*, Integrated sound software, 1998.

[12] E. Larsson, *A domain decomposition method for the Helmholtz equation in a multilayer domain*, SIAM J. Sci. Comput., 20 (1999), pp. 1713–1731.

[13] E. Larsson, *Domain Decomposition and Preconditioned Iterative Methods for the Helmholtz Equation*, PhD thesis, Department of Information Technology, Uppsala University, 2000.

[14] E. Larsson and S. Holmgren, *Parallel solution of the Helmholtz equation in a multilayer domain*, BIT, 43 (2003), pp. 387-411.

[15] J. Liu and Q. H. Liu, *A spectral integral method (SIM) for periodic and nonperiodic structures*, IEEE Microwave and wireless components letters, vol. 14 (2004), No. 3.

[16] S. Marburg, B. Nolte, *Computational Acoustics of Sound Propagation in Fluids. Finite and Boundary Element Methods*, Springer Verlag, Berlin Heidelberg New York, 2008.

[17] P. M. Morse and H. Feshbach, *Methods of Theoretical Physics*, McGraw–Hill, New York, 1953.

[18] K. Otto, *Iterative solution of the Helmholtz equation by a fourth-order method*, Boll. Geof. Teor. Appl., 40:1 suppl. (1999), pp. 104–105.

[19] K. Otto and E. Larsson, *Iterative solution of the Helmholtz equation by a second-order method*, SIAM J. Matrix Anal. Appl., 21 (1999), pp. 209–229.

[20] J. G. Papastavridis, *Tensor Calculus and Analytical Dynamics*, CRC Press, Boca Raton, FL, 1999.

[21] E. Sundkvist and K. Otto, *Discretization of a hybrid model for acoustic wave propagation in layered fluid media*, Technical report 2011-15, Department of Information Technology, Uppsala University, 2011.

[22] E. Turkel, A. Yefet, *Absorbing PML boundary layers for wave-like equations*, Applied Numerical Mathematics, 27:4(1998), pp. 533-557.

[23] V. V. Varadan, A. Lakhtakia, and V. K. Varadan, eds., *Acoustic, Electromagnetic, and Elastic Wave Scattering*, vol. 1, Elsevier Science Publishers, Amsterdam, The Netherlands, 1991.

[24] O. Von Estorff, ed., *Boundary elements in acoustics: Advances and applications*, WIT Press, Southampton, 2000.

[25] T. W. Wu, ed., *Boundary element acoustics: Fundamentals and computer codes*, WIT Press, Southampton, 2000.

[26] L. C. Wrobel, *The Boundary Element Method. Volume 1. Applications in thermo-fluids and acoustics*, John Wiley&Sons, LTD, 2002.